Aeroacoustics Conferences
June 14-17, 2022, Southampton, UK
28th AIAA/CEAS Aeroacoustics 2022 Conference

10.2514/6.2022-2807

An Approach towards semi-empirical Slat Track Noise Prediction

Michael Pott-Pollenske[1], Meike Jansen[2]
Deutsches Zentrum für Luft- und Raumfahrt e.V.,38108 Braunschweig, Germany

High lift wing leading edge noise is often attributed to the slats or more generally speaking to the leading edge high lift device. Except for droop noses, flow exposed mechanical systems are necessary to mount and actuate such devices. For mechanical reasons these so called "tracks" are typically oriented perpendicular to the wing leading edge and accordingly inclined towards the mean flow or flight direction. Mainly from wind tunnel studies and in rare cases also from flight tests these tracks are known as strong noise sources, which locally exceed slat noise levels and show up as intense noise sources in noise maps originating from phased array beamforming. This finally means that track noise cannot be omitted for the noise prediction of high lift systems and in particular not in view of new systems like Krueger flaps. Against this background track noise was investigated in the German national funded research project INTONE (Minderung von Triebwerksinstallations- und Hochauftriebslaerm). Based on parametric studies with the small scale DLR F16 high lift system in DLR's Acoustic Wind Tunnel Braunschweig track noise was isolated and characterized. In a second step a first prediction scheme was established. The scheme allows now for the prediction of slat noise and track noise and the summation of both components which contributes to the overall leading edge noise. The application of this model showed the impact and importance of track noise compared to slat noise. Furthermore, the noise generation at the D-nose cut-outs was assessed. Both results together reveal that track noise is a major contributor to the overall high lift system noise and track noise reduction is essential in order to reduce the high lift system related airframe noise contribution. The current development is meant as first step towards a more sophisticate tool chain for wing leading edge noise prediction.

Nomenclature

a	=	speed of sound, [m/s]
c_p	=	pressure coefficient
c_s	=	slat chord length, [m]
F(f,M)	=	spectral shape function
Δf	=	analysis bandwidth, [Hz]
f_m	=	1/3-octave band centre frequency, [Hz]
I	=	integral of the spectral shape function
L_{corr}	=	normalized sound pressure level, [dB]
ΔL_{geo}	=	sound pressure level difference related to size, [dB]
ΔL_{total}	=	sum of sound pressure levels, [dB]
ΔL_v	=	flow or flight speed related sound pressure level difference, [dB]
ΔL_x	=	sound pressure level correction for polar directivity, [dB]
ΔL_y	=	sound pressure level correction for azimuthal directivity, [dB]

[1] Research Eng., Inst. of Aerodynamic and Flow Technology, michael.pott-pollenske@dlr.de
[2] Research Eng., Inst. of Aerodynamic and Flow Technology, meike.jansen@dlr.de

M = free flow Mach number
M_{Pred} = Mach number for track noise prediction
p' = acoustic pressure, [Pa]
SPL = sound pressure level re $20*10^{-6}$ Pa, [dB]
SPL_{norm} = normalized sound pressure level, [dB]
St = Strouhal number
S_s = span, [m]
u = velocity, [m/s]
U_{inf} = free stream velocity, [m/s]
U_{span} = flow velocity in spanwise direction, [m/s]
x, y = positions in wind tunnel or flight test coordinate system, [m]
α = aerodynamic angle of attack, [°]
α_{geo} = geometrical angle of attack, [°]
β = sweep angle, [°]
Γ = amplitude function
μ_n = numerical constants for spectral function (n = 0,1,2,3)
σ_n = auxiliary constants in spectral function (n = 0,1,2,3)

Abbreviations

AWB = Acoustic Wind Tunnel Braunschweig of DLR
DNW = German-Dutch Wind Tunnels
NWB = Low Speed Acoustic Facility of DNW in Braunschweig
PROFAN = PRediction MOdel For Airframe Noise

I. Introduction

The noise generated at the leading edge of current high lift systems can be understood as superposition of multiple noise sources as visualized in Fig. 1 on the example of the Airbus A320 wing. Generally speaking, leading edge noise is dominated by slat noise and slat track noise. Slightly less important but still prominent are edge noise sources in particular at the inner slat and the pylon intersection. Other sources like e.g. de-icing pipes, seals or rubber joints are negligible for the overall airframe noise contribution and prediction.

For real aircraft slat track noise is regarded as superposition of noise generated at the tracks itself and noise related to the interaction of turbulent flow with the openings in the main wing leading edge. Fast semi-empirical noise prediction tools based on aircraft flyover noise and wind tunnel data like e.g. DLR's PROFAN[1] are typically not able to distinguish between all three sources and merge them altogether in "slat noise" which in fact represents high lift system leading edge noise. In contrary, analytical models, such as the one developed by Guo[2], are able to predict slat noise in a precise manner but do not account for the influence of slat tracks on wing leading edge noise.

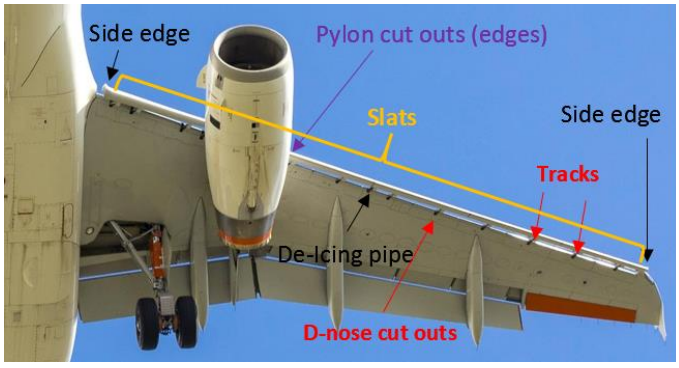

Fig. 1: Assembly of wing leading edge related noise sources

The present paper summarizes the development of a noise prediction scheme for both slat noise and slat track noise. The work is mainly based on model scale wind tunnel experiments conducted in DLR's Acoustic Wind Tunnel in Braunschweig with the DLR F16 high lift wing under different operating conditions. The new model is checked against the current PROFAN prediction which is based on wind tunnel and flight test data. Finally, the contribution of the track cut-outs to real aircraft slat noise is worked out on basis of flyover noise data as acquired for an Airbus A319 aircraft with open and closed D-nose track cut-outs.

II. Small Scale Experimental Study

A. Scope and Test Setup

The scope of the wind tunnel study was to quantify the noise generated by one single slat track installed on a high lift system. A number of slat tracks featuring different shapes and degrees of details were assessed in the course of the German national funded research project INTONE (Minderung von Triebwerksinstallations- und Hochauftriebslaerm). For basic research purposes a generic slat track was specifically designed and used for the present work (Fig. 2). The track is depicted without the sealing plate that can be added on the small rectangular surface (red arrow in Fig. 2). This slat track served exclusively as acoustic source and did not support the slat mechanically.

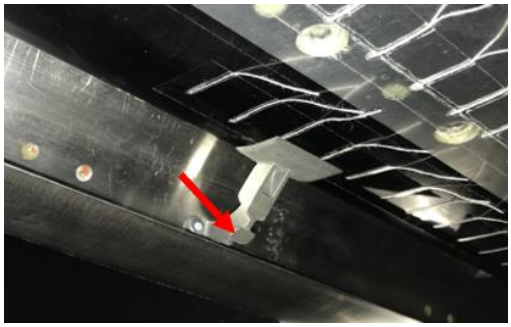

Fig. 2: Generic slat track

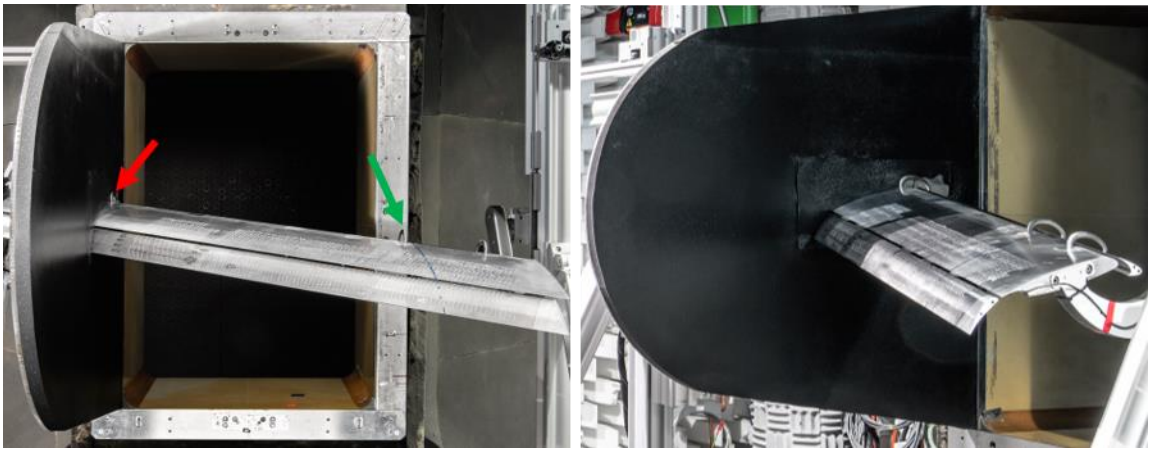

Fig. 3: F16 model setup in AWB. Left: upstream view. Right: side view

An overview of the test setup is provided in Fig. 3. On the left hand side of Fig. 3 the high lift wing is shown in an upstream view showing the flow oriented slat brackets close to the side wall (left, red arrow) and right apart of the vertical shear layer of the wind tunnel nozzle on the open wing end (green arrow). The long spanwise distance of about 900 mm between the suction side brackets ensures the least degree of noise contamination by those brackets.

The high lift system was installed with a fixed 30° sweep angle while the angle of attack could be adjusted. A specialty of the setup is the asymmetry. It turned out that a second side plate, shielding also the rear end of the high lift system against the wind tunnel shea layer, led to massive flow separations affecting up to one third of the entire span. In the finally chosen open rear wing end configuration no separations occurred. This aerodynamic benefit was accepted for the disadvantage of a weak excess noise source due to the interaction of the wing with the turbulent shear layer.

All tests were conducted for wind speeds of 40, 50 and 61.5 m/s. The highest wind speed of 61.5 m/s relates to a Reynolds number of about 1 Mio based on the 300 mm stowed chord of the DLR F16 high lift system. The majority of all test data was acquired for an aerodynamic angle of attack of 6° which relates to a geometric angle of attack of 14°.

The aerodynamic validation and correction were based on the comparison of measured static surface pressures in a mid span cross section of the high lift system to measurement data of a closed section wind tunnel and a computation of the entire setup in AWB. The comparison of test data and computation is presented in Fig. 4 and shows a good collapse of both data set. The selected aerodynamic design point represents well a typical condition for aircraft in approach was varied by about ±2° within the test. The variations did not show remarkable aerodynamic or acoustic effects. For this reason, the paper will focus on data as acquired for the target aerodynamic angle of attack of 6° and the mentioned flow speeds.

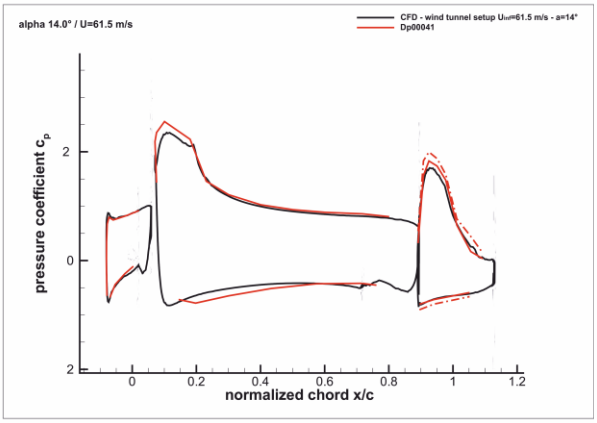

Fig. 4: Comparison of computed and measured static surface pressure distribution in a mid span cross section of the F16 high lift system for a free stream velocity of 61.5 m/s and a geometrical angle of attack of α=14°

B. Wind Tunnel Test Results

The acoustic assessment of the high lift system was mainly based on phased array beamforming with the 96 microphone AWB microphone array. Conventional beamforming and CLEAN-SC[3] were applied for different scan areas in order to first identify and rank order noise sources and second to derive spectral representations of both slat noise and slat track noise. Additionally, single microphone farfield noise data were acquired. The analysis of these farfield noise data revealed that a clear identification and characterization of slat track noise generated at this single track is impossible due to a very poor signal to noise ratio between the test cases with and without slat track. Accordingly, the final acoustic analysis is based on phased array microphone data.

In the following noise source maps as acquired with and without track are presented. The single track was installed at position x~0.45 m and y~0.1 m. The following figures represent the noise sources as obtained by conventional beamforming for the reference wing without track (left in each plot) and with track (center plot). On the right hand side a CLEAN-SC beamforming result for the configuration with track is visualized. All data refer to a flow speed of U_{inf} = 61.5 m/s and an aerodynamic angle of attack of 6°.

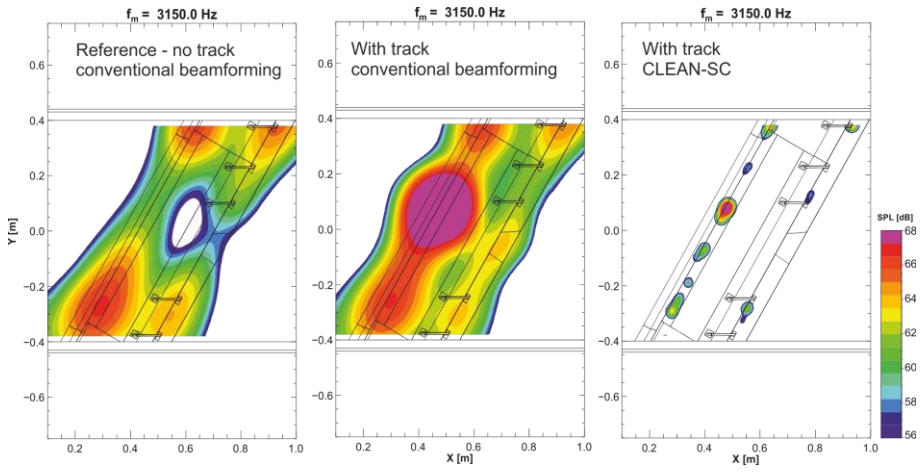

Fig. 5: Acoustic source plots for the 3150 Hz 1/3-octave band

In Fig. 5 noise source plots are depicted for a 1/3-octave band frequency of 3150 Hz. For the reference wing (left) strongest sources can be seen at the wall junction (x = 0.25 m, y = -0.4m) and for the wing-shear layer interaction

(x = 0.55 m, y = 0.4 m). The related maximum sound pressure levels are about 64 – 66 dB. Adding the track (centre plot, x = 0.45 m, y = 0.1 m) led to a new and even stronger source of at least 68 dB for this 1/3-octave band. All aforementioned sources remain constant. The relatively poor spatial resolution of the array causes the quasi mixture of the side wall junction source with the track source itself. A much clearer view provides the data processing with the CLEAN-SC algorithm which reveals the track to be the dominant noise source. Please note that both dynamic range and levels are similar in all source plots.

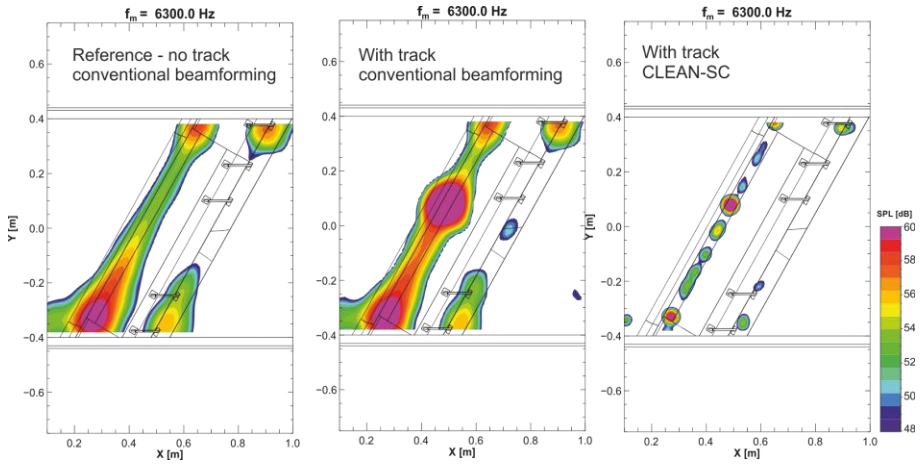

Fig. 6: Acoustic source plots for the 6300 Hz 1/3-octave band

Somehow similar source plots were computed for the 6300 Hz 1/3-octave band depicted in Fig. 6. Again, the side wall junction and the shear layer interaction show up as most relevant sources for the reference configuration without slat track. The presence of the track led to a new and again strongest source (centre plot) that can be precisely localized and identified by means of the CLEAN-SC processing (right plot).

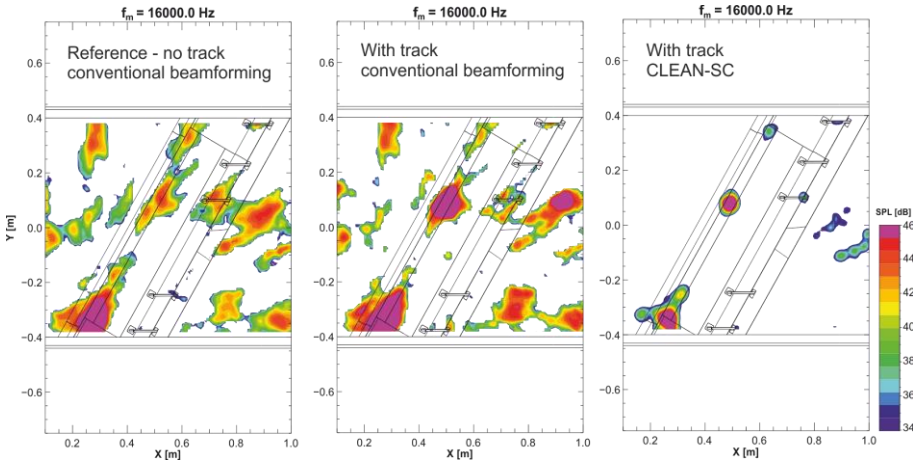

Fig. 7: Acoustic source plots for the 16000 Hz 1/3-octave band

For the high frequency 16 kHz 1/3-octave band similar findings can be noted (Fig. 7). Even though the conventional beamforming starts to suffer from sidelobes contaminating the source plot the slat track is clearly identified by both the conventional beamforming and the CLEAN-SC processing.

The results obtained proof that one track can be identified and isolated on the high lift wing and that excess noise sources were identified. Track noise and excess noise can be separated be either suitable scan grids or the application of appropriate array processing tools. In a second step of the data analysis a slat focused scan area was defined. The size of this new grid was adopted in order to assess the slat track together with a representative portion of slat span.

The resulting noise maps for the final grid are exemplified in Fig. 8 for the 6300 Hz 1/3-octave band. As can be seen, the entire slat track source is captured in the grid area (right hand side) while the slat noise levels remain constant over nearly the entire span (left hand side) as should be expected in this case. These noise source plots can be considered representing the slat source and the combination of slat and track noise. Accordingly, in a first attempt the source power integration method was used to extract integrated narrow band sound pressure level spectra representing the two sources of interest.

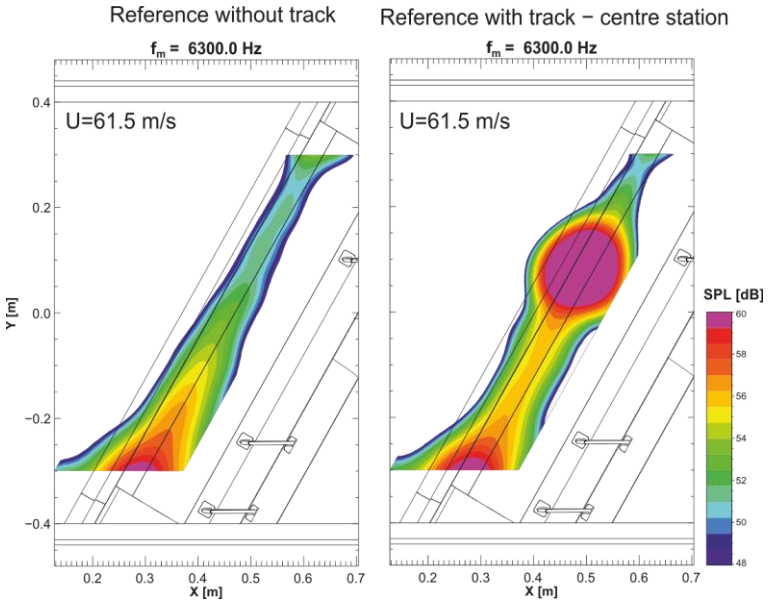

Fig. 8: Acoustic source plots as processed for the small adopted scan grid and a 1/3-octave band frequency of 6300 Hz

The integrated spectra are plotted in Fig. 9 in terms of narrowband sound pressure levels for the three wind speeds of 40, 50 and 61.5 m/s in blue, red and green line colour. Bold lines represent track and slat noise (track installed) while thin lines show the result for the slat only test cases without track.

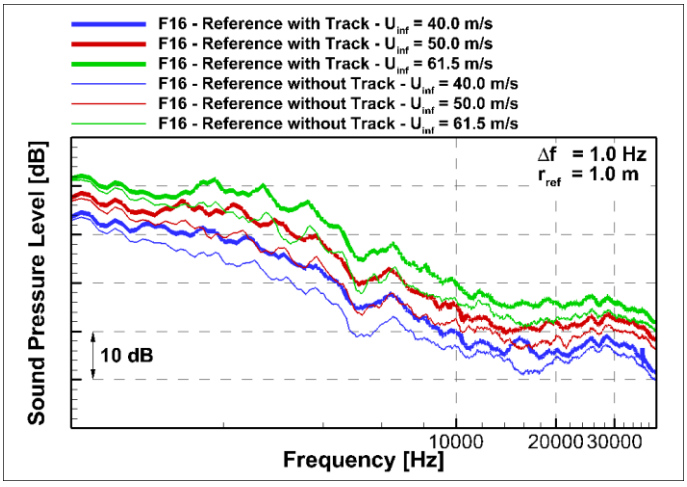

Fig. 9: Sound pressure level spectra representing slat and track noise

Generally speaking, the two sets of sound pressure level spectra show similar levels for very low frequencies below 1000 Hz. These results are most likely related to low frequency shear layer oscillations and wind tunnel background noise. Track and slat related spectra separate from each other at frequencies of about 1000 Hz showing a continuous level roll off for up to maximum frequencies of about 30 kHz. The sound pressure levels drop for even higher frequencies. The track related data exhibit level maxima at frequencies of about 2 kHz. All spectra show a level dip at frequencies of about 5 kHz. At this frequency the spectra dived in two parts. For the frequency domain below 5 kHz both, a Strouhal number scaling and a typical $p'^2 \sim u^5$ velocity power law are observed. For frequencies above 5 kHz only the sound pressure levels are still a function of the wind speed and follow a velocity law slightly above u^5. The level differences obtained for the three flow speeds are quite similar. This finding indicates velocity power laws of the same order of magnitude for both noise sources.

III. Track Noise Prediction Approach

The main rationale of the approach is to establish a prediction of slat noise and slat track noise based on the model data acquired in the course of the already mentioned INTONE study. Once a scheme is available it shall be tested for predictions of other test cases such as different wind tunnel models or full scale predictions like e.g. from the existing and established PROFAN scheme.

A. Slat Noise Prediction

Very briefly summarized Guo's model provides a shape functions for the sound pressure level spectrum and the directivity of slat noise as function of the Strouhal number. The methodology and functions used by Guo for the prediction of slat noise are presented and explained in detail in Ref. [2]. At this point a brief summary of selected basic equations used from Guo's work for the purpose of this study is listed in the following section.

The power spectral density is expressed as function of the Mach number and the Strouhal number. Equation (69) of Ref. [2] reads:

$$\langle p'^2 \rangle = \frac{M^2}{2 \cdot I(M)} \cdot \sum_{n=0}^{2} \frac{\Gamma_n}{\sigma_3^2 + \sigma_n^2} \left[\sigma_n \cdot \pi + \sigma_3 \cdot ln \frac{\sigma_3^2}{\sigma_n^2} \right] \text{ with} \tag{1}$$

Γ_n and σ_n being auxiliary constants and *I(M)* representing the integrated spectral shape function F for the slat noise power spectral density (equation (52) in Ref. [2]), which is a function of both the frequency and Mach number and reads:

$$F(f, M) = \frac{M^2 \cdot c_S}{a} \cdot \frac{St^2}{(1+\mu_0^2 St^2) \cdot (1+\mu_1^2 \cdot (1+M^2) \cdot St^2) \cdot (1+\mu_2^2 \cdot M^2 St^2) \cdot (1+\mu_3 \cdot M \cdot St)} \tag{2}$$

The Strouhal number *St* is defined according

$$St = \frac{f_m \cdot c_S}{U_{inf}}. \tag{3}$$

with the slat chord length representing the source dimension and the free stream or flight speed U_{inf}.

In contrast to PROFAN the Guo model as documented in Ref [2] does not provide a calibration for absolute sound pressure levels. Therefore, the systematic used in PROFAN will be adapted to calibrate the shape function in order to fit to the obtained experimental data.

The calibration is based on a source dimension ratio *F* defined as the slat area divided by a unit area according to

$$F = \frac{\frac{c_S * \cos(\beta)}{S_S}}{(1.0 \cdot 1.0\ m^2)}. \tag{4}$$

The respective sound pressure level correction reads

$$\Delta L_{geo} = 10 \cdot \log_{10}(F). \tag{5}$$

The directivity functions ΔL_x and ΔL_y were also taken over from PROFAN. The respective definitions can be obtained from Ref. [1] and Ref. [4] with detailed explanations. A constant level correction of ΔL_{corr} = 60.0 dB completes the overall level calibration that reads

$$\Delta L_{total} = \Delta L_{corr} + \Delta L_{geo} + \Delta L_x + \Delta L_y. \tag{6}$$

The reference slat noise spectrum as obtained from the aforementioned experimental dataset was finally compared to a slat spectrum as computed with Guo's shape function and the documented calibration on basis of the geometrical and operational data of the experiments. The comparison of both spectra is depicted in terms of narrow band sound pressure level spectra for all tested flow speeds in Fig. 10. As can be seen, the spectra match reasonably well for frequencies between 1 kHz and 10 kHz. Within this frequency range differences of less than 1 dB exhibit for the lowest flow speed of U_{inf} = 40 m/s. Slightly higher deviations occur for the flow speed of U_{inf} = 50 m/s and even higher differences show up for the highest flow speed of U_{inf} = 61.5 m/s. The reason for this systematic deviation is probably a small difference in the velocity power law. While the test data follow a $p'^2 \sim u^{4.5}$ power law Guo's model is based on a u^5-velocty law.

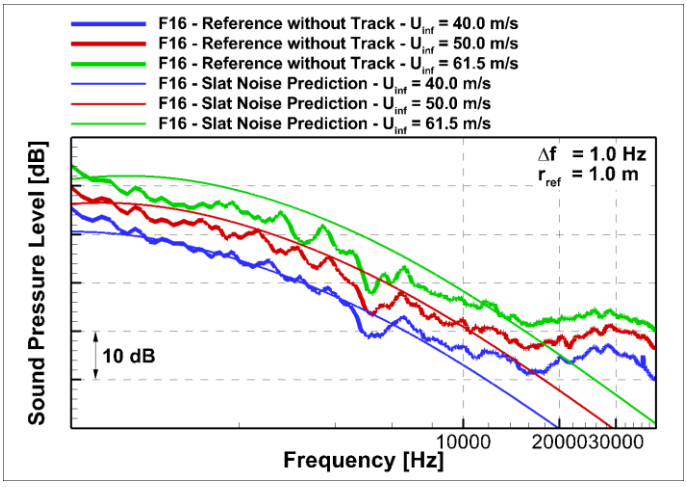

Fig. 10: Comparison of measured and predicted slat noise spectra for all three flow speeds

Remarkable differences between measurement and prediction exhibit for frequencies higher than 10 kHz. While the slat shape function shows a continuous level roll off the test data exhibit a relative level minimum at about 16 kHz frequency, an increase up to 30 kHz and final level roll off for even higher frequencies. Respective noise maps indicate noise generated at the slat leading edge for frequencies higher than 16 kHz which could potentially contribute here among other weak excess noise sources that sum up to the visualized data. However, these sources do not represent slat noise in the sense of Guo's model and accordingly they cannot be predicted with this model. The achieved result can be considered satisfactory for the scope of this work and accordingly it will be used in the further development of a slat track noise prediction method. It is worth to mention that the spectra presented in Fig. 10 do not simply end at a frequency of about 800 Hz. In fact the predicted slat noise data follows the given shape function while the measured data turn over from model generated noise to low frequency wind tunnel background noise.

B. The Characteristics of Slat Track Noise

Slat track noise is extracted from the available data by means of an energetic subtraction of the integrated spectra obtained for the reference configuration and the test case with the slat track installed. The subtraction is carried out on narrow band spectra. This is possible, because the spectra do not include strong tonal components that would deteriorate the final spectra. The result of the subtraction is shown in Fig. 11 for the highest flow speed of U_{inf} = 61.5 m/s.

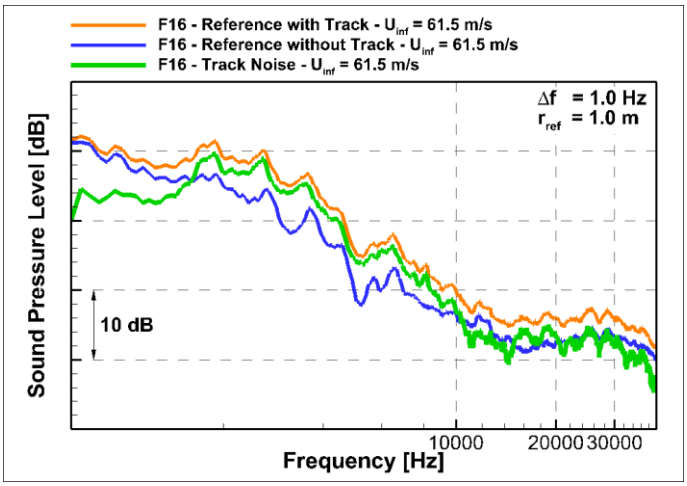

Fig. 11: Spectral representation of track noise for one generic slat track on the F16 high lift system

The orange and blue curves represent the initial data for slat and slat track. Accordingly, the green curve shows the resulting sound pressure level spectrum for one generic slat track on the F16 high lift system. The resulting spectra for all other wind speed were derived in the same manner. A collection of all three spectra for wind speeds of 40, 50 and 61.5 m/s are depicted in Fig. 12.

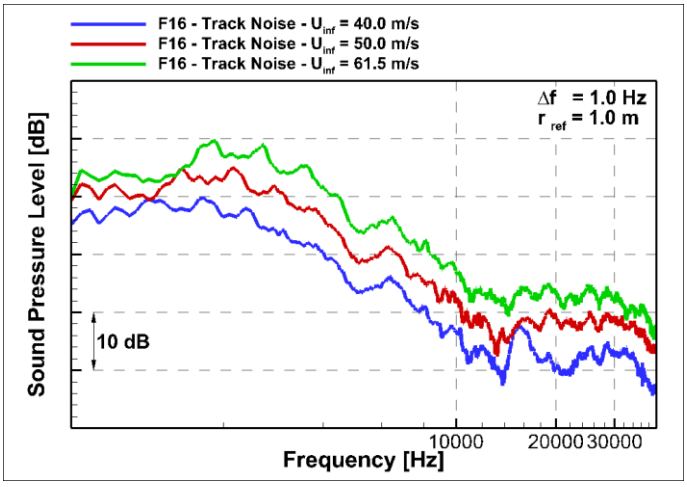

Fig. 12: Track noise spectra plotted versus frequency as derived for three flow speeds by means of energetic subtraction

Based on the presented data the spectra exhibit two major characteristics. First, maximum levels occur for low frequencies of about 2 kHz, a first level roll off ends at frequencies of approx. 5 kHz. Within this low frequency domain both, levels and frequency scale with the flow speed according to a u^5-power law. The second and high

frequency part of the spectra begins at about 5 kHz and shows a Helmholtz number scaling. The respective sound pressure levels still follow the u^5 velocity law. These findings are depicted in Fig. 13 in terms of track noise sound pressure level spectra as obtained for the three wind speeds and plotted versus Strouhal number as dimensionless frequency.

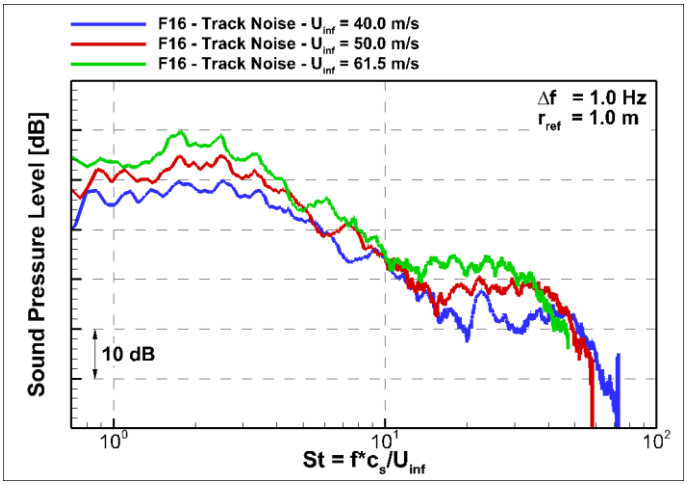

Fig. 13: Track noise spectra plotted versus Strouhal number as derived for three flow speeds by means of energetic subtraction

C. The Track Noise Prediction Scheme

The analysis of track noise characteristics revealed the qualitative similarity of fundamental scaling laws for low frequency slat and track noise. This led to the hypothesis that the governing noise generation mechanism could also be similar. If we state that the acceleration of turbulent flow and its convection past the slat trailing edge represent the dominant source mechanism of slat noise, the similar flow features should be connected to track noise.

This analogy seems to hold true when analyzing mean flow data from flow computations. The RANS-computations were achieved with the DLR TAU code and encompassed the entire wind tunnel setup for the tested slat track configurations. The mean flow field at the track station is presented in Fig. 14. On the left hand side of Fig. 14 the slat track is omitted. In this case the typical and expected flow field around the main wing leading edge and in the slat gap is computed. The light blue colour indicates the position of the stagnation line in the slat cove. With the track

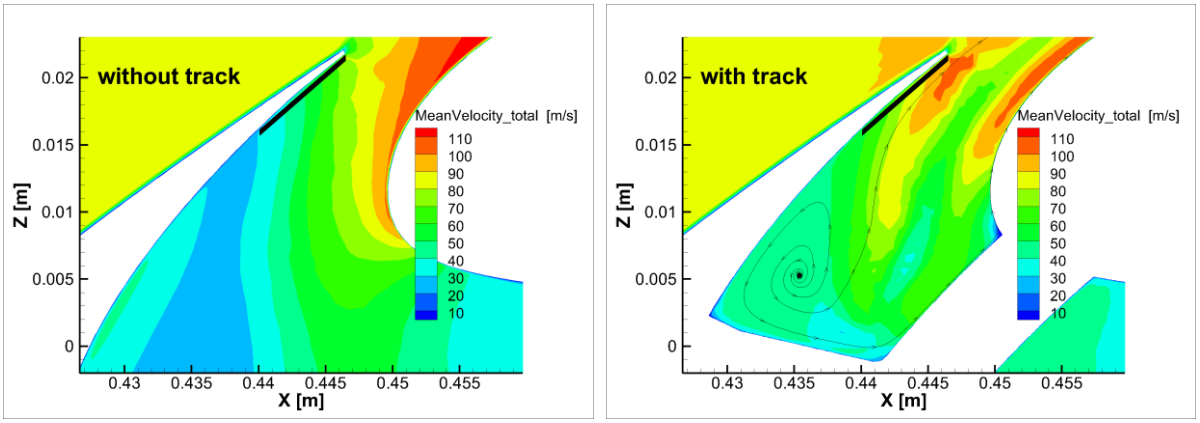

Fig. 14: Mean flow field in the slat gap without (left) and with (right) slat track.

respected (Fig. 14, right hand side, same colour code) one cannot see the stagnation line, which is obvious by the fact

that the track prevents the emergence of the large slat cove vortex. Instead, a smaller vortex is generated in the kink between track and slat cove which feeds turbulence into the flow field. Furthermore, flow speeds in the vicinity of the slat trailing edge are higher than for the case without track. This is explained by a stronger acceleration of the flow which also includes a stronger turbulence acceleration in this flow regime. Based on these findings an adaptation of Guo's prediction scheme seems reasonable for the prediction of low frequency track noise. In a first attempt the flow speed increase will be respected for the track noise prediction. Therefore, flow speeds were averaged over the extend of the black line indicated at the slat trailing edge. It turned out that flow speeds with track are about 1.444 times higher than without track. This ratio will be implemented in Guo's scheme in order to derive a suitable flow Mach number M_{Pred}, defined as

$$M_{Pred} = \frac{1.444 \cdot U_{inf}}{a} \tag{7}$$

The low-frequency part of the track noise spectrum will be determined for a portion of the span over which an influence of the track is determined. The latter is not a strong criterion and was evaluated based on engineering judgement and the computed static pressure distribution around the track. It turned out that left and right from the track a span of about 0.04 m, in absolute dimensions only valid for the F16 model, is affected by strong track related pressure and velocity gradients. Since this is for now the only available data to assess the "span" of the track this zone of influence is considered representative for the track span and thus used for the track noise prediction.

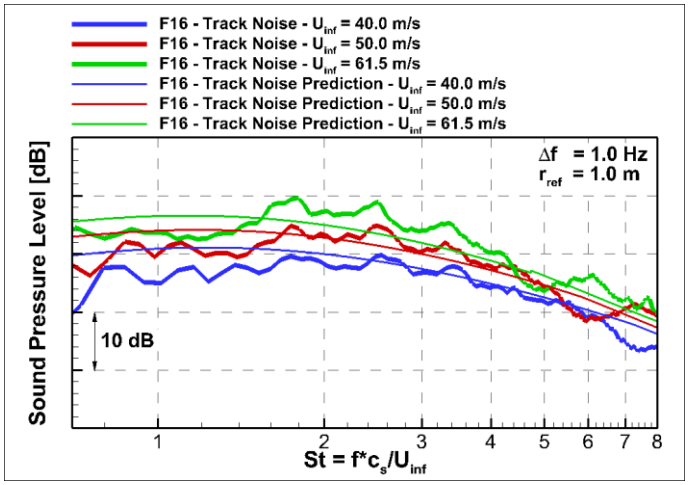

Fig. 15: Comparison of low frequency track noise spectra as measured (bold solid lines) and predicted (thin lines)

The low frequency prediction result for all flow speeds is given in Fig. 15 in terms of the measured and predicted narrow band sound pressure level spectra plotted versus the Strouhal number. A reasonable data fit is observed for the lower flow speeds of 40 and 50 m/s and a Strouhl number range of $2 < St < 5$. The larger offset visible for U_{inf} = 61.5 m/s, which is in fact in the order of about 2 dB, is (i) caused by bigger humps in the measured data and (ii) an effect of the underlaying velocity dependence. However, this initial prediction result for low frequency slat track noise is considered satisfactory and proves the selected approach in general.

As mentioned, the Strouhal number scaling turns over to a Helmholtz number scaling at a frequency of 5 kHz for the regarded model. This means, the low frequency data needs to be cut off at the Strouhal number corresponding to a frequency of 5 kHz. In a second step, the high frequency part of the spectrum must be predicted and added in order to predict a complete track noise spectrum.

Before the prediction approach is explained it is worth to discuss in brief the dominating noise generation mechanism. One early hypothesis was that the flow along the span and therefore both, the flow impingement on the tracks and the flow separation at the tracks represent one governing noise source mechanism. A small experiment showed that this assumption is at least reasonable but perhaps incomplete. During the experiment pressurized air was blown out of a nozzle along the span of the slat without any mean flow around the model as visible in Fig. 16. The

flow speeds were adjusted to levels in the order of $U_{span} = U_{inf}$*sin(β) and measured by a small anemometer for a direct comparison to the so far discussed experimental database.

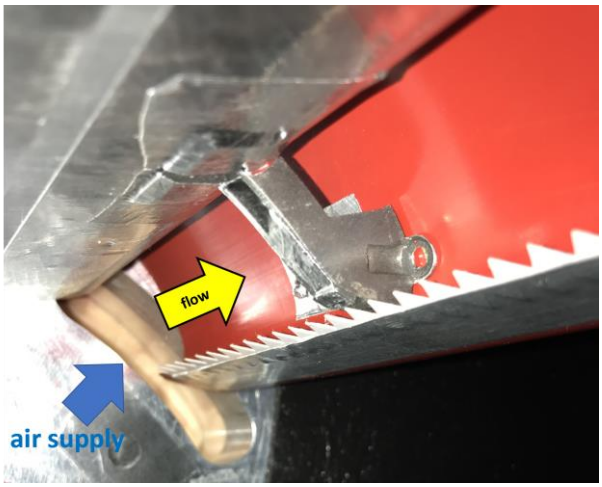

Fig. 17: Side experiment to determine to effect of spanwise flow on track noise

The remaining spectra, of course, differ and one could speculate that the free stream inflow on the high lift system is at least one reason causing this noise. However, this simple experiment supports the hypothesis that the high frequency part of track noise is predominantly generated by the spanwise flow component.

The prediction of the high frequency track noise component is based on a simple polynomial approximation. The shape was derived from the spectra presented in Fig. 18. It turned out that a 4th grade polynom achieves the best fit and thus serves for the prediction.

The final polynom reads

$$SPL(f) = A \cdot f^4 - B \cdot f^3 + C \cdot f^2 - D \cdot f + k \qquad (8)$$

with the coefficients
A = 5.97e-17
B = -7.905e-12
C = 3.479e-07
D = -0.006188;

and k as velocity function defined as

$$k = 70.86 - 50 \cdot log_{10}\left(\frac{100.00}{U_{inf}}\right) [dB] \qquad (9)$$

The results of the experiment are depicted in Fig. 17. The blue curve represents the track noise data derive from the F16 experiment for a wind speed of U_{inf} = 50 m/s. This data is first compared to the red curve highlighting narrow band sound pressure level spectra as obtained for a flow speed of 25 m/s in span direction which is the theoretical spanwise flow speed for U_{inf} = 50 m/s under sweep of β = 30°. In particular for the frequency range up to 10 kHz the spectral shape looks similar. The blue and red arrows in Fig. 17 mark a peak in the spectrum. The frequency ratio of the peaks is about 1.04 which is considered negligible and compensated for the green curve which was at the same time shifted upwards to fit the peak levels. Now a nice collapse of this peak and the spectrum up to an upper frequency limit of about 10 kHz can be observed.

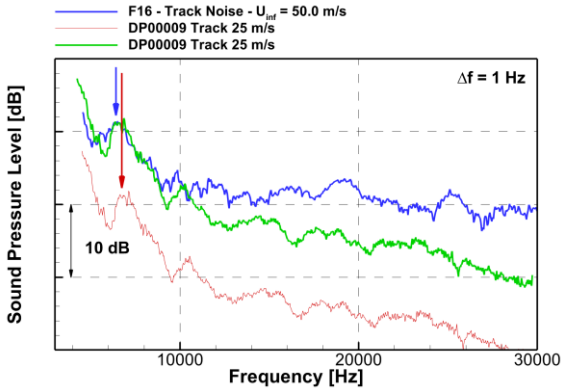

Fig. 16: Comparison of narrow band sound pressure level spectra from the side experiment and the F16 study

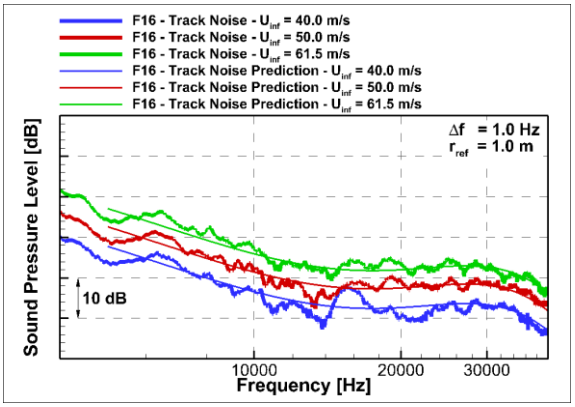

Fig. 18: Summary of high frequency track noise spectra with a polynomial approximation for each spectrum

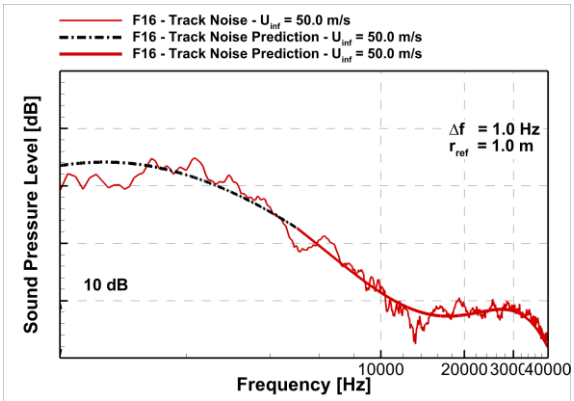

Fig. 19: Final track noise prediction as composed of the low frequency and the high frequency spectral component

The finally predicted track spectrum (Fig. 19) is composed in the frequency domain by transposing the low frequency part from Strouhal number to frequency. The definition of the junction between the LF and HF part follows the given equations and provides a smooth transition from LF (black curve) to HF data (red curve) as can be seen in Fig. 19.

Based on the individual predictions slat and track data were energetically superimposed and compared to the respective measurement data for all tested flow speeds. The result is depicted in terms of narrow band sound pressure level spectra in Fig. 20. The presented data reveal a good collapse of measurement and prediction over almost the entire frequency range. Difference worth to mention show up for very high frequencies above 16 kHz. This shortcoming can be accepted because the respective pressures are about 30 dB below the maximum levels and have therefore only limited relevance for real life application.

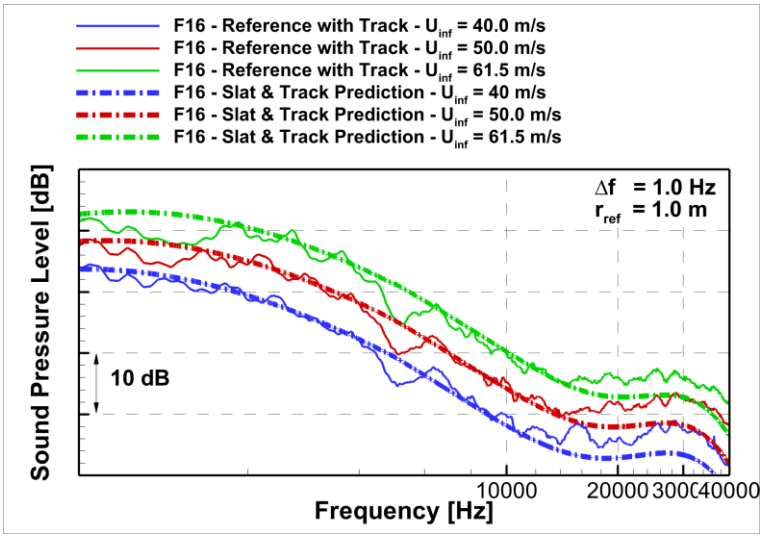

Fig. 20: Comparison of measured and predicted LE noise spectra

D. Application to Full Scale Aircraft Noise Prediction

Due to missing suitable experimental data a cross check for validation of the developed prediction method is not feasible. Most experimental setups suffer from insufficient free span width in order to determine an uncontaminated slat noise spectrum and additionally the respective data with an installed slat track.

A. Slat and Slat track Noise Prediction

Instead, the new method will be applied to the prediction of full scale aircraft data, namely the prediction of Airbus A320 slat and slat track noise. This widely operated aircraft served for the development of the PROFAN prediction scheme at DLR[5] and was up to now used for airframe noise research. As can be seen in Fig. 1, the slat of this aircraft can be divided in three segments. Segment 1 is the inner slat between the fuselage and the engine. This slat element is supported by 4 tracks. Segment 2 is the slat element outboard of the engine. It's spanwise extend is defined up to the outboard flap side edge. This element is supported by 6 slat tracks. Last but not least the outboard element supported by two tracks is segment 3. The following Table 1 lists all elements, their span and the number of supporting tracks.

Table 1: Slat segments and dimensions

	Span [m]	Number of supporting tracks
Segment 1	4.575	4
Segmemt 2	6.9	6
Segment 3	2.85	2

The predictions were carried out for a flight speed of U_{inf} = 66.9 m/s and the high lift system configuration with full deflected slats and flaps. All noise data are referenced to a 1 m propagation distance and will be presented in terms of 1/3-octave band sound pressure level spectra. The PROFAN slat noise prediction, which is known to fit reasonably well to the A320 slat noise data, serves as reference for comparison.

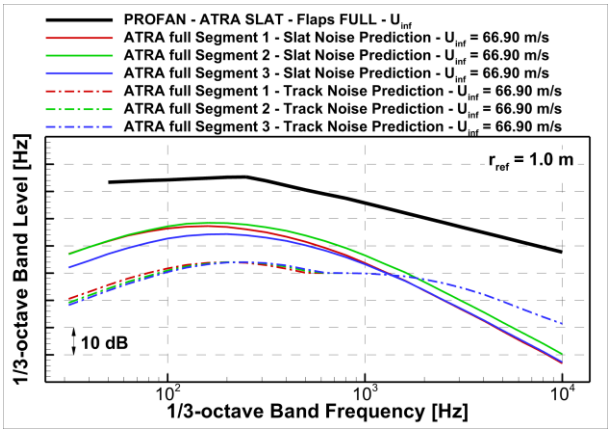

Fig. 21: Full scale slat and track noise prediction per segment and track

The initial prediction was carried out for each slat segment and one track at each segment. The results are depicted in Fig. 21. As can be seen, the different tracks, represented by the dashed dotted lines, do not show remarkable level differences, what in fact could be expected. The slat segments, represented by solid lines, show reasonable differences. The longest slat segment no. 2 (green curve) shows highest noise levels while the short segment no. 3 is predicted with lowest pressure levels.

In a second step slat and track noise were energetically added. The spectra for each slat segment and the respective number of supporting tracks are depicted in Fig. 22. The effect on slat and track noise is twofold. In the low frequency domain a marginal noise level increase of about 1 dB is noted. This effect is explained by the large pressure level difference of low frequency slat and track noise which is at the end not compensated by the number of tracks. In the mid and high frequency domain a significant noise level increase of up to 10 dB for segment 2 can be observed.

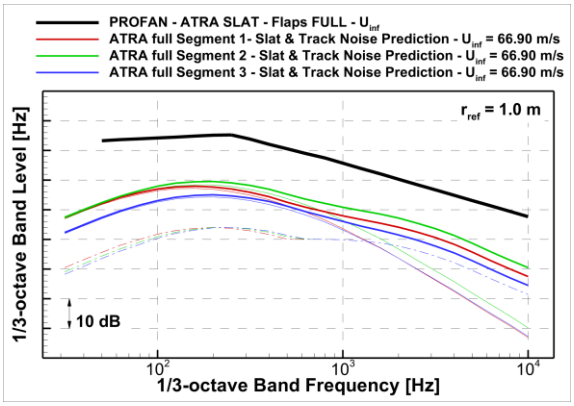

Fig. 22: Impact of tracks on slat noise

The final step is now to double and sum up the components in order to derive a slat noise spectrum for the complete aircraft. This final prediction result differs much in terms of pure levels from the so-called reference (Fig. 23). The main reasons for this have already been mentioned in the introduction. A prediction based on farfield noise data generated by full or semi span aircraft models accounts implicitly for more noise sources than slat and slat track noise as for instance edge noise sources. This effect is represented by the present data set. Furthermore, the real H-shape track shapes and other details cannot be modeled in detail with a semi-empirical scheme but tend to increase noise levels. The used wind tunnel models feature smooth geometries and do not account for the above mentioned effects which explains the observed level differences.

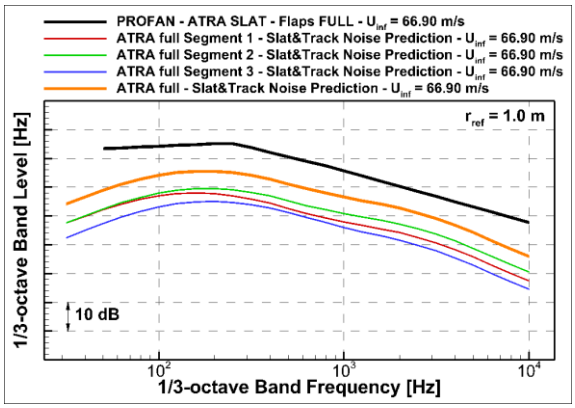

Fig. 23: Comparison of slat noise predictions based on the PROFAN scheme and the new method

On the other hand and much more important is the fact that the spectral shape is captured very well by the new method. It proves that even the model type geometries are suitable to generate relevant and characteristic sound pressure level spectra that can be used to establish prediction schemes as well as noise reduction technologies.

B. Importance of D-Nose Cut-outs

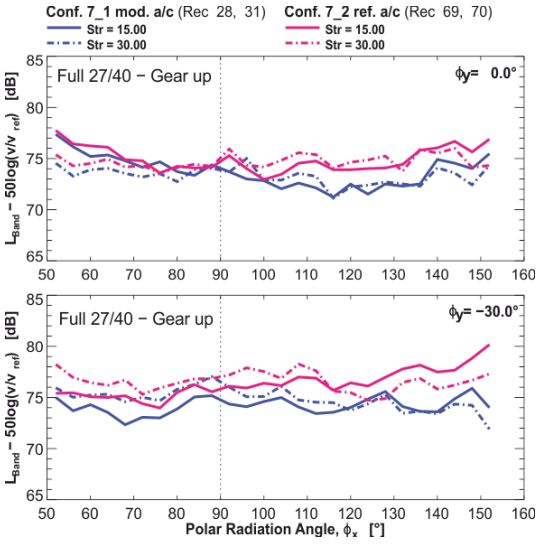

Fig. 24: Polar noise radiation for closed and open D-nose slat track cut-outs for lateral observer positions of φ_y = 0° and φ_y = 30°.

Excess noise generated at D-nose cut-outs cannot be evaluated on basis of experimental data because they simply do not exist, at least at DLR. However, data from flight tests carried out with Lufthansa in the year 2001 are available and were evaluated[6]. The Airbus A319 test aircraft flew a set of flyovers with closed cut-outs on the first test day and with open cut-outs on the second day. A description of the test setup and the applied data analysis is provided in Ref. [6]. At this point it should be emphasized that all noise data were de-Dopplerized and corrected according to international standards[7], in particular the atmospheric absorption was considered according to the correction scheme of Bass and Sutherland[8]. The deeper analysis of these data revealed that noise generated at the track cut-outs contribute to the overall airframe noise signature for frequencies between 2 kHz and 4 kHz. As the polar noise directivity plots depicted in Fig. 24 show, the noise level increase with open cut-out can be quantified with about 2 dB. This finding is valid for lateral noise radiation angles φ_y between 0° (centerline) and 30°. Even though this contribution does not affect the maximum noise level, which is at lower frequencies, it contributes significant to A-weighted or perceived noise data and thus might have an influence on certification levels. This data supports well the argumentation given in the last paragraph., Adding up these data to the given prediction the difference at high frequencies reduces to about 3 to 4 dB. Furthermore, the data proves the necessity to perform either large scale test with highly detailed models or, more complicated and expensive, flight tests with suitable measurement techniques to assess also single noise sources.

IV. Conclusion

Within the reported study a prediction method for slat and slat track noise was developed. The prediction method was tested step by step against measurement data obtained with the DLR F16 high lift system.

The study showed thereby one method to predict slat and slat track noise individually and at the same time to assess the effect of their combination. The latter showed clearly the significant influence of track noise on slat noise which should better be called wing leading edge noise, because the same mechanisms could occur for a Krueger leading edge device.

The prediction test of a full scale aircraft showed the ability of the method to predict slat related leading edge noise in terms of its spectral shape. At the same time absolute sound pressures are underpredicted. The main reasons for this shortcoming are named and can be added to refine te method which is and will be under development for the next future. The presented side study in D-nose cut out noise supports this rationale.

The presented work is considered as starting point for the development of a more sophisticated tool that will allow for a more detailed high lift system noise prediction as current state of the art semi-empirical methods.

Acknowledgement

The reported work was part of the German national research project INTONE (Minderung von Triebwerksinstallations- und Hochauftriebslaerm) funded by the German Federal Ministry for Economic Affairs and Energy.

The author thanks all colleagues from Airbus who contributed to this work.

References

[1] Dobrzynski, W., Almoneit, D., Rossignol, K.-S.:" Handbuch zum modularen Quellmodell".

[2] GUO, Yueping: "Aircraft Slat Noise Modeling and Prediction", AIAA Paper No. 2010-3838, 16th AIAA/CEAS Aeroacoustics Conference 07 June 2010 - 09 June 2010, Stockholm, Sweden, https://doi.org/10.2514/6.2010-3837.

[3] Sijtsma, P., "CLEAN Based on Spatial Source Coherence", 13th AIAA/CEAS Aeroacoustics Conference, 21 May 2007 - 23 May 2007, Rome, Italy, https://doi.org/10.2514/6.2007-3436.

[4] Pott-Pollenske, M., Dobrzynski. W., Buchholz, H., Guerin, S., Saueressig, G., Finke, U.: „Airframe Noise Characteristics from Flyover Measurements and Predictions", 12th AIAA/CEAS Aeroacoustics Conference (27th AIAA Aeroacoustics Conference), 08 May 2006 - 10 May 2006, Cambridge, Massachusetts, https://doi.org/10.2514/6.2006-2567.

[5] Pott-Pollenske, M., Dobrzynski, W., Buchholz, H., Gehlhar, B., Walle, F.:" Validation of a Semiempirical Airframe Noise Prediction Method through Dedicated A319 Flyover Noise Measurements", AIAA 2002-2470, 8th AIAA/CEAS Aeroacoustics Conference, 17-19 June 2002, Breckenridge, Colorado / USA.

[6] Pott-Pollenske, M., Dobrzynski, W., Buchholz, H., Gehlhar, B., Walle, F.:" Validation of a Semiempirical Airframe Noise Prediction Method through Dedicated A319 Flyover Noise Measurements", AIAA 2002-2470, 8th AIAA/CEAS Aeroacoustics Conference, 17-19 June 2002, Breckenridge, Colorado / USA.

[7] International Standards and Recommended Practices, Environmental Protection, Annex 16 to the Convention on International Civil Aviation, Volume 1, Aircraft Noise.

[8] Bass, H.E., Sutherland, L.C., Zuckerwar, A.J.: "Atmospheric Absorption of Sound: Update", J. Acoust. Soc. Am. 88(4), pp. 2019-2021, Oct. 1990.